CCS Observations of the Protostellar Envelope of 11335

T. Velusamy, T. B. H. Kuiper, W. D. Langer

Jet Propulsion Laboratory, California Institute of Technology, Pasadena, CA 91 109

Received _____, accepted _____

ABSTRACT

We present single dish and interferometric spectral line observations of CCS at 22 GHz towards the core of B335, a classical example of a young protostellar region. We combined the VLA and DSN 70-m observations to produce high resolution (6" and 1.2") channel maps at 0.04 km s^{-1} velocity intervals. These maps image for the first time the collapsing envelope around the protostar. These show that CCS emission arises primarily from the outer parts of the collapsing envelope down to half the infall radius and that CCS is clumpy throughout the core. LVG excitation analysis indicates that X(CCS) is $\sim 3 \times 10^{-9}$ in the outer envelope and $< 5 \times 10^{-11}$ in the center of the infall region. The absence of CCS in the interior could be due to time dependent chemical evolution. The velocity structure supports the evidence for inside-out collapse and the high velocity features are consistent with accretion onto a rotating central disk. The asymmetric clumpy distribution of CCS emission implies that the physical conditions are not spherically symmetric, and that the gas falling onto the circumstellar disk may be episodic.

Subject headings: protostar formation - molecular cloud cores - molecules

1. Introduction

Knowledge of the density, velocity and chemical profiles around protostars is of fundamental importance for testing dynamical models of protostar evolution and understanding the nature of the material falling onto circumstellar disks. B335 is one of the best studied classical examples of a young, low mass stellar object with a bipolar outflow (Frerking & Langer 1982) and infall (Zhou et al. 1993). In this *Letter* we report the first direct imaging of the infall by combining single dish and interferometric observations. We present CCS observations and narrow velocity channel (0.04 km s^{-1}) maps of the core and the infalling envelope. CCS is an ideal probe for such studies because it is comparable to CS in requiring relatively high density ($\sim 10^4$ - 10^5 cm^{-3}) to excite, has an intrinsically narrow line width (0.09 km s^{-1} at 10 K), but unlike the cyanopolyynes, has no hyperfine structure. It is thus well suited for resolving kinematical details. We combined NASA Goldstone 70-m single dish and VLA interferometric observations of CCS to resolve the small scale structure surrounding the central object. This approach is extremely powerful because it can provide direct images at different velocities to bring out the dynamical structure of both large and small scale features.

Chandrasekhar (1939) showed that an isothermal cloud which is in equilibrium between thermal pressure and self-gravity will have a density structure of the form r^{-2}. Shu (1977) found that the fluid equations also allowed a non-static solution, in which the gas collapses onto the center with an infall velocity which is proportional to $r^{-0.5}$, resulting in a density structure proportional to $r^{-1.5}$ in the region of collapse. Both the infall velocity and the density scale as the square root of the mass of the central core, which grows linearly with time. The infall region is therefore described entirely by its age, or equivalently its core mass, or the radius of the outer edge of the infall region (age x sound speed). This simple model was surprisingly effective in describing the CS emission and H_2CO absorption

observations in the central region of B335 (Zhou et al.] 993). These lines consist of a blue peak at 8.1 km s^{-1} and a smaller red peak at 8.5 km s^{-1}. A Monte Carlo radiative transfer model of inside-out collapse fits even better (Choi et al. 1 995). The outer radius of the in-fall region is 0,030 pc (25") and the mass of the central core is 0.4 $M_\odot$. The age of the infall is 1 .5× 105 yr and the accretion rate is 2.S × 10-'6 $M_\odot$ yr^{-1}. Zhou et al. (1 993) conclude that B335 is a true protostar, i.e. it derives its luminosity only from the conversion of gravitational energy.

The overall morphology of the B335 region is described by Frerking, Langer & Wilson (19S7). The size and velocity of the bipolar outflow imply an age of about 1- 4 x 10^5 yr. Moriarty-Schieven and Snell (1989), using a mean outflow velocity corrected for inclination, favor the lower time estimate. It should be noted that the presence of a bipolar outflow does not conflict with the. collapse model, since the outflow occupies only 13 percent of the solid angle (Zhou et al. 1993).

The central region was detected in the infrared by Keene et al. (1 983), and consists of a cold (15 K) compact (<30") core of far-l]{ emission with an even smaller, warmer ($\geq$25 K) center. Chandler and Sargent (1 993) partially resolved the opaque core in 2.7 mm continuum emission, which they found to be about 1000 AU long oriented along a position angle of 20° east of north, but less than 500 AU perpendicular to that axis, with a mass of 0.2 $M_\odot$. Velocity-integrated ^{13}CO emission is centered on this object and extends along a position angle of 120°. Their evidence for bipolar outflow on this scale is easily recognize] when compared to larger scale maps, such as those of Hirano et al (1 992). They conclude ' that the molecular outflow can be traced to within '250 AU of the source.

2. Observations

We made single dish maps of B335 in the 22 GHz CCS $J_N = 2_1$-1_0 transition with high signal-to-noise, Nyquist sampling every 24" over a 4' × 4' region around the position of the CS J=5-4 peak (Zhou et al. 1993) at RA(1950) =19"34'''35'.25 and DEC(1 950) = 7°27'30". For the CCS transition we usc 22344 .033 MHz (Yamamoto et al. 1990; Pickett, Poynter & Cohen 1991). The observations were made between 1993 May and 1994 June, using NASA's DSN 70 m-antenna at Goldstone, California, for about 100 hours total integration. At 22 GHz, the aperture efficiency was about 40 percent, the antenna HPBW is 45". The pointing accuracy was limited by a cyclic hour angle error with an amplitude of 5.5" and a period of 1.4° (5.6 rein) which results in a slight smearing of the beam to at most 50". The pointing was checked observing the radio source DR 21. The receiver consisted of a maser pre-amplifier followed by a digitally-controlled Hewlett-Packard down-converter with a synthesized local oscillator locked to the station hydrogen maser frequency standard, The system has a noise temperature of 50 K measured at the zenith. We used the two million (22') channel Wide Band Spectrum Analyzer (Quirk et al. 1988) with a spectral resolution of 19 Hz over 40 MHz. The resolution was reduced by co-adding 32 adjacent channels to provide 8192 channels of 610 Hz (0.008 km S-l) resolution. The spectra were observed in position switching mode and were 1)oppler corrected to an accuracy of about 0.004 km s^{-1}.

The VLA CCS spectral line maps at 22 GHz were made in D-configuration on 1995 Feb 22-23 and March 2 for 18 hours total integration, with velocity resolution $\sim$ 0.041 km s^{-1}. Data were taken using 256 channels and 0.78 MHz bandwidth, without Hanning smoothing. The source 1947+ 079 (flux density 0.474 Jy at 22,3 GHz) was used for amplitude and phase calibration. 3C48 was used as the primary calibrator for flux density and passband calibration.

3. Results

Figure 1 shows the spectrum of the 22 GHz CCS transition observed with an effective 50″ beam centered on the 1 R source. The beam is comparable to the infall region. The line has a width near the base: ~0.5 km s^{-1} and consists of two peaks separated by approximately 0.2 km s-', This line is in all respects narrower than the CS and H_2CO lines observed by Zhou et al (1993). This implies that the CCS emission comes from the outer envelope as discussed in more detail below.

The mean velocity, which also corresponds to the velocity of the central minimum, is 8.383±0.005 km s^{-1}, is slightly different from the 8.35 km s^{-1} value assumed by Zhou et al. (1993). Here we will take S,3S km s^{-1} to be the rest velocity of B335, as suggested by the CCS spectrum. Figure 1 also shows the 22 GHz VLA spectrum at the central position obtained from the channel maps smoothed to a resolution of 1 5" which corresponds to about one third the size of the infall region. The VLA spectrum shows two distinct peaks with a velocity separation of 0.43 km s^{-1}. These features can only be seen weakly, if at all, in the wings of the single dish spectrum because of beam dilution. The minimum in the VLA spectrum near S.4 km s^{-1} is not an absorption feature. Rather it results from the *absence* of CCS at low velocities near the center of an extended emission region which is resolved out by the VLA.

As the 70-m antenna beam is comparable to the size of the infall region, we used the VLA data to study the structure at smaller scales. The shortest spacing in the VLA was about 2500 λ and hence, in the VLA maps structures on the scale of 30" and larger are missing. The 70-m maps contain all spatial frequencies up to about 4000 λ. In Figure 2 (*Plate*) we show an example of a channel map at V_{LSR} = 8.4 km s^{-1} obtained with the DSN 70-m and the VLA. The negative feature at the center of the VLA map (which is also seen in the VL A spectrum in Figure 1 at this velocity) is actually an absence of emission (a hole) in the middle of an extended (~ 60") brightness distribution. This extended emission cannot be detected in the VLA map because of the missing short spacings in the VI, A data.

To overcome this limitation we have combined the 70-m and VLA data to produce high fidelity images such as shown in Figure 2c. The 70-m maps were made in the exact channel frequencies and widths to match the VLA channels. The visibilities derived from the single dish maps were added to the VLA visibilities to produce the maps shown in Figure 3. (The details will be discussed in a subsequent paper.) The combined maps were smoothed to a $19'' \times 12''$ beam to improve the signal-to-noise. The velocity spacing of the maps in Figure 3 is slightly less than the Nyquist spacing; because the velocity resolution is limited by the thermal line width which amounts to 0.10 km s^{-1} for CCS at 12 K. In each map, the circle shows the radius (25″) of the infall region derived by Choi et al. (1995). The diagonal line inside the circle shows the orientation of the central disk seen at 2.7 mm (Chandler & Sargent). Outside the circle the CO bipolar outflow is outlined as in Zhou et al.

At the rest velocity of 8.38 km s^{-1}, and in the adjacent maps, the CCS emission region is about 2' NS by 1.5' EW. We will refer to the channel maps by their Doppler shift relative to the source rest velocity of 8.38 km s^{-1}. The most striking feature in Figure 3 is the minimum in the brightness distribution near the center of the infall region which is evident from -0.04 to +0.08 km s^{-1}. As seen in Figure 2 this feature is too small to be resolved with the 70-m antenna while the surrounding emission is resolved out in the VLA data and only the combined map brings out the true structure.

In Figure 3 the brightest emission is seen at +0.21 km s^{-1} (V_{LSR}=8.6 km s^{-1}). The emission at this velocity has sufficient brightness to enable us to use a higher resolution of 6″. In this highest resolution map (Figure 4) two prominent features are seen, one within the infall circle and the second just outside in the NW. The emission within the infall circle is elongated in the SW to NE direction. Interestingly at red shifts of +0.17 km s^{-1} and 0.21 km s^{-1} one of the bright spots is located near the NE edge of the central continuum disk. There is also an emission peak, albeit weaker, at a blue shift of -0.12 km s^{-1} displaced towards the SW along the orientation of the disk (Figure 3). These are consistent with

infalling material converging onto the periphery of the central disk. Such a velocity field is indicative of rotation about an axis pointing to the east. 'i'his result is consistent with the sense of rotation inferred by Zhou (1 995) from the variation of CS line shapes inside the infall region.

Finally, the CCS emission is clumpy. There are a number of emission peaks just at or outside of the boundary of the infall region. They are comparable in size to, or slightly larger than, the 12" resolution limit of the map. Some have peculiar velocities with respect to the infall center. Notable are those, seen to the south in the -0.08 and -0.04 km s^{-1} maps, and the prominent clump at the infall circle to the northwest at +0.17 to +0.25 km s--', This distribution suggests that the core of B335 has the same kind of subsonic, clumpy strut.tum seen in TMC-1 core D (Langer et al 1995). Most of the ones which are not at the boundary of the infall region appear to *avoid* the CO outflow region mapped by Hirano et al (1992).

4. Discussion

Overall, our CCS data provide good support for tile inside-out collapse model in B335. Compared to the profiles of CS and H_2CO, the narrower separation of the maxima of the central CCS profile implies an absence of CCS in the central region where the infall velocities are highest. The model of Choi et al. (Figure 5) shows that< gas with a radial velocity of ± 0.1 km s^{-1} with respect to the central velocity is at a distance of $\sim$ 0.020 pc (18") from the center along the line of sight, whereas ± 0.2 km s^{-1} gas is at $\sim$ 0.015 pc (12"), In the VLA spectrum and channel maps (Figures 1 & 3) the highest infall velocity of CCS is only $\sim \pm 0.2$ km s^{-1}. As seen from Figure 5 this suggests that CCS is present only in the outer envelope down to half the infall radius. The channel maps confirm the general absence of CCS inside the core at low relative LSR velocities,

CCS requires relatively high density to excite (Langer et al 1 995) and, since the density is higher towards the center, the absence of emission in the center must be due to a lack of CCS. Note that the reason for the central hole in CCS is different from the one proposed for the hole in the H_2CO absorption map by Zhou et al (1 990). This hole represents a region near the center of the core where the H_2CO absorption at 6 cm is suppressed by the higher densities there. We can estimate the fractional abundance of CCS, X(CCS), using an LVG excitation model and recent quantum calculations for the collision rate coefficients (Wolkovitch et al. 1995). We have high resolution observations for only the one $J=2_1-1_0$ transition at 22 GHz and so adopt the density and temperature profiles for the infall region from Choi et al. (1995). Furthermore, the excitation analysis indicates that the 22 GHz line is not optically thick ($\tau < 1$), similar to the results derived for TMC 1 using multi-transition analysis (Langer et al. 1995). The 22 GHz CCS brightness ($T_b \sim$ 1.5-3 K) for the infall envelope in the, VLA maps yields a $X(CCS) \sim 3 \times 10^{-9}$ for densities $\sim$ a few x 10^{5} cm^{-3}. The limits on T_b (< 0.5 K) for CCS emission in the VLA maps and the fact the density is higher by one to two orders of magnitude close to the infall center ("hole") place an upper limit there of 5×10^{-11} for X(CCS). Clearly there is a void in CCS abundance inside the infall region and hence the velocity structure of CCS traces the kinematics of the envelope of the infall region.

The lack of CCS emission in the inner 10" cannot be due to the absence of gas and dust at the center, as continuum measurements and models of the H_2CO and CS line profiles indicate that the average density increases towards the center. Instead, we believe, that the explanation lies in the chemical properties of CCS. A lack of CCS could either be due to depletion at the higher densities found in the central region or to CCS being a tracer of early time chemistry. There is evidence in HL Tau for depletion of CS during the evolution from the protostellar core to a. dense disk (Blake, van Dishoeck & Sargent 1992). However, the disk of HL Tau is of considerably higher density than the central 10" of B335. The

major problem with the depletion model in the case of CCS in B335 is that CS and H_2CO should deplete to a similar degree (Bergin, Langer & Goldsmith 1995) and yet the line formation models of Zhou et al. indicate that these are present throughout the inside-out collapse region. It would appear that the best explanation lies in the evolutionary models of molecules in collapsing cores (cf. Rawlings et al. 1992 who model the evolution of a number of molecules, but not CCS). It seems likely, that CCS is characteristic of early time ($t \leq 10^5$ yr) chemistry (Millar & Herbst 1990, Suzuki et al. 1992, Hirahara et al. 1992). In this case CCS is produced recently, in the dense gas being formed as a result of the collapse of the core, and destroyed in the oldest and densest material which is in the central region. Hence, on average CCS is more prominent in the exter ior, less evolved regions than other molecules which" have longer survival times. The rate of chemical evolution depends on the physical conditions of the gas, to which CCS is more sensitive than other molecules. The clumpy structure of CCS, which is also evident in the TMC-1 core D (Langer et al. 1995), is thus attributed to variations in these conditions in the core of B335.

in summary, the transient nature of CCS enabled us to observe phenomena which would be hidden by more widespread tracers. We found from CCS interferometric and single dish observations of B335 that CCS is largely absent in the central 10", and that CCS appears to occur primarily in the region just outside the infalling envelope. The CCS distribution is clumpy, rather than smoothly varying, both in the infalling envelope and the surrounding cloud. The location and velocity of clumps seen near the center of the core are consistent with a rotation axis pointing to the east. Overall, the CCS emission supports the infall model of Shu et al, and the previous observations of Zhou and co-workers. Because our CCS observations show that the infalling material is clumpy rather than smoothly varying, the infall onto the circumstellar disk may be episodic. The consequences of such an infall model have yet to be explored in terms of the evolutionary history of the disk.

We thank Drs. C. Chandler and V. Migenes for help in the VLA observations, the

Goldstone Complex staff and particularly the Radio Astronomy and Radar Group for support of the 70-m observations, Dr. J. Keene for insights suggested by her unpublished observations, and Dr. D. Koerner for useful discussions regarding rotating disks. This research was conducted while '1'. V. held a US National Research Council - Senior Resident Research Associateship. This work was performed at the Jet Propulsion Laboratory, California Institute of Technology, under contract with the National Aeronautics and Space Administration. The VLA of the National Radio Astronomy Observatory is operated by Associated Universities Inc. under contract with the NSF.

REFERENCES

Bergin, E. A., Langer, W. D. & Goldsmith, P. F. 1995, ApJ 441, 222.

Blake, G. A., van Dishoeck, E. F. & Sargent, A. 1992, ApJ 391, L99.

Chandler, C. J. & Sargent, A. I. 1993, ApJ 414, L29.

Chandrasekhar, S. 1939, An Introduction to the Study of Stellar Structure (Chicago: U. Chicago Press).

Choi, M., Evans, N. J., 11, Gregersen, E. M. & Wang, Y. 1995, ApJ, in press.

Frerking, M. A. & Langer, W. D. 1982, ApJ 256, 523.

Frerking, M. A., Langer, W. D. & Wilson, R. W. 1987, ApJ 313, 320.

Hirahara, Y., Suzuki, H., Yamamoto, S., Kawaguchi, K., Kaifu, N., Ohishi, M., Takano, S., Ishikawa, S. & Masuda, A. 1992, ApJ, 394, 539

Hirano, N., Kameya, O., Kasuga, T. & Umemoto, T. 1992, ApJ 390, 1,S5.

Keene, J., Davidson, J. A., Harper, D. A., Hildebrand, R. H., Jaffe, D. T., Lowenstein, R. F., Low, F. J. & Pernic, R. 1983, ApJ 274, 1,43.

Langer, W. D., Velusamy, 'T'., Kuiper, T. B. H., Levin, S., Olsen, E. T., & Migenes, V. 1995, ApJ (in press)

Millar, 'T', J. & Herbst, E. 1990, A&A 231, 466.

Moriarty-Schieven, G. H. & Snell, R. L. 19S9, ApJ 338, 952.

Pickett, H., Poynter, R. & Cohen, E. 1991, Submillimeter, Millimeter and Microwave Line Catalog: Revision 3. Jet Propulsion Laboratory.

Quirk, M. D., Wilk, H. F., Garyantes, M. F. Grimm, M. J. 19S8, IEEE Trans. on Acoustics, Speech & Signal Processing; 36, 1854.

Rawlings, J. M. C., Hartquist, 'T'. W., Menten, K. M. & Williams, D. A. 1992, MNRAS 255, 471.

Shu, F. 11.1977, Ap.J J. 214, 48S.

Suzuki, H., Yamamoto, S., Ohishi, M., Kaifu, N., Ishikawa, S.-i., Hirahara, Y. & Takano, S. 1992, ApJ 392, 551.

Wolkovitch, D., Goldsmith, P. F., Langer, W. D., Kuiper, T. B. H., Heyer, M., Velusamy, T., & Levin, S., 1995, in preparation.

Yamamoto, S., Saito, S., Kawaguchi, K., Chikada, Y., Suzuki, 11., Kaifu, N. & Ohishi, M. 1990, ApJ 361, 318.

Zhou, S. 1995, ApJ 442, 685.

Zhou, S., Evans, N. J., II, Kömpe, C. & Walmsley, C. M. 1993, ApJ 404, 232.

This manuscript was prepared with the AAS LaTeX macros v3.0.

Fig. 1.- The 22 GHz CCS spectra observed with the DSN 70-m antenna and the VLA (from channel maps smoothed to 15" resolution) at the central position of B335. The velocity resolution is 0.00S km s^{-1} and 0.04 km s^{-1} respectively, for the DSN and VLA spectra. The negative intensity near $V_{LSR} = 8.4$ km s^{-1} in the VIA spectrum is the result of missing short-spacings (see text).

Fig. 2.— Channel maps of 22 GHz CCS emission of the B335 core at $V_{LSR} = 8.3$ km S-* and channel width 0,04 km s^{-1} observed with (*a*) DSN 70-m, (*b*) VLA-D configuration, and (c) obtained by combining the 70-m and VI, A data. The angular resolution in the VLA maps is 12", The beam sizes are indicated by the circle in the lower right corner of the maps. The contour intervals are 0.09, 0.26 and 0.35 K in T_b respectively for the 70-m, VLA and combined maps. The circle near the center of the maps represents the infall region of the protstellar collapse. Note that prior to combining with the VLA data the 70-m map was attenuated by the VLA primary beam (2') and the VLA and combined maps shown here arc not corrected for primary beam.

Fig. 3.-– Channel maps of 22 GHz CCS emission made by combining the Goldstone and VLA data. The velocity of each channel is labeled with respect to the rest velocity, V_{LSR} = 8.38 km s^{-1}. The velocity width of the channels is 0.0409 km S-l. The spatial resolution in the maps is 12"x12". The lowest contour level and contour interval are 20 mJy beam-l (0.35 K in T_b); the rms noise in the map is 13 mJy beam-l. The infall region and the orientation of the disk are marked by the central circle and line respectively. The outflow lobes mapped in ^{12}CO by Hirano et al. (1992) are shown by solid (blue shifted) and clashed (red shifted) lines.

Fig. 4---- High resolution (6") single channel map of $+0.21$ km s^{-1} emission. The lowest contour level and contour interval are 12 mJy $beam^{-1}$ (0.84 K in T_b); the rms noise in the map is 9 mJy $beam^{-1}$, Other details are the same as for Figure 2.

Fig. 5---- Contours of equal line-of-sight velocity of the infall, projected on a plane which contains both the source and the observer. The model parameters are taken from Choi et al (1995). The velocity spectrum of the CCS emission at any offset position from the center is determined by the relative contribution of the V_Z contours integrated along the line of sight.

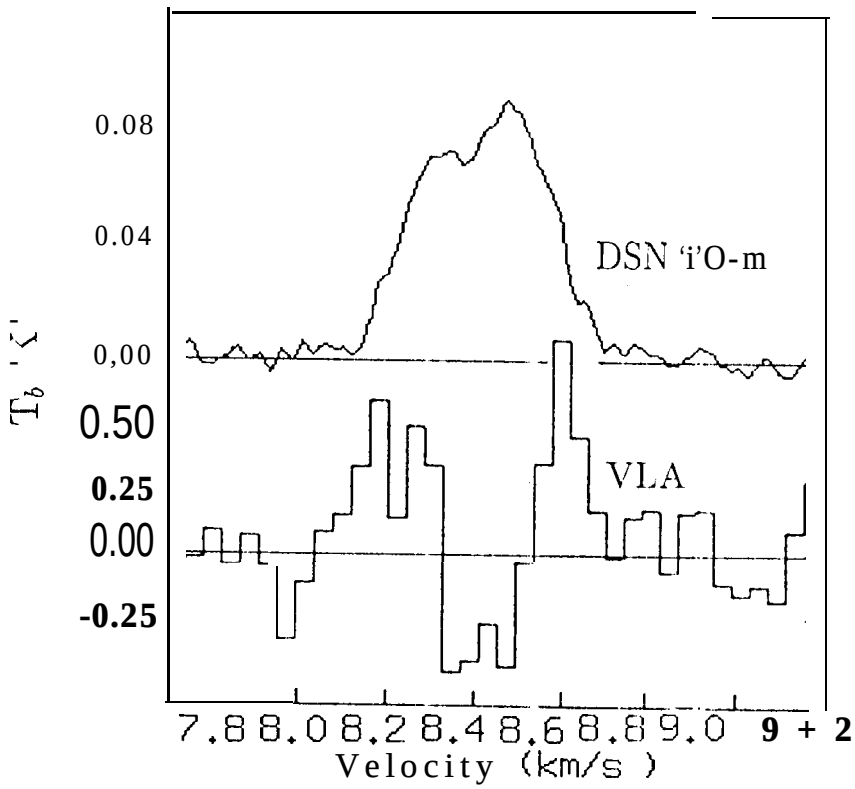
0.08
0.04
0,00
0.50
0.25
0.00
-0.25
DSN 'i'O-m
VLA
7.8 8.0 8.2 8.4 8.6 8.8 9.0 9 + 2
Velocity (km/s)

Pig. 1

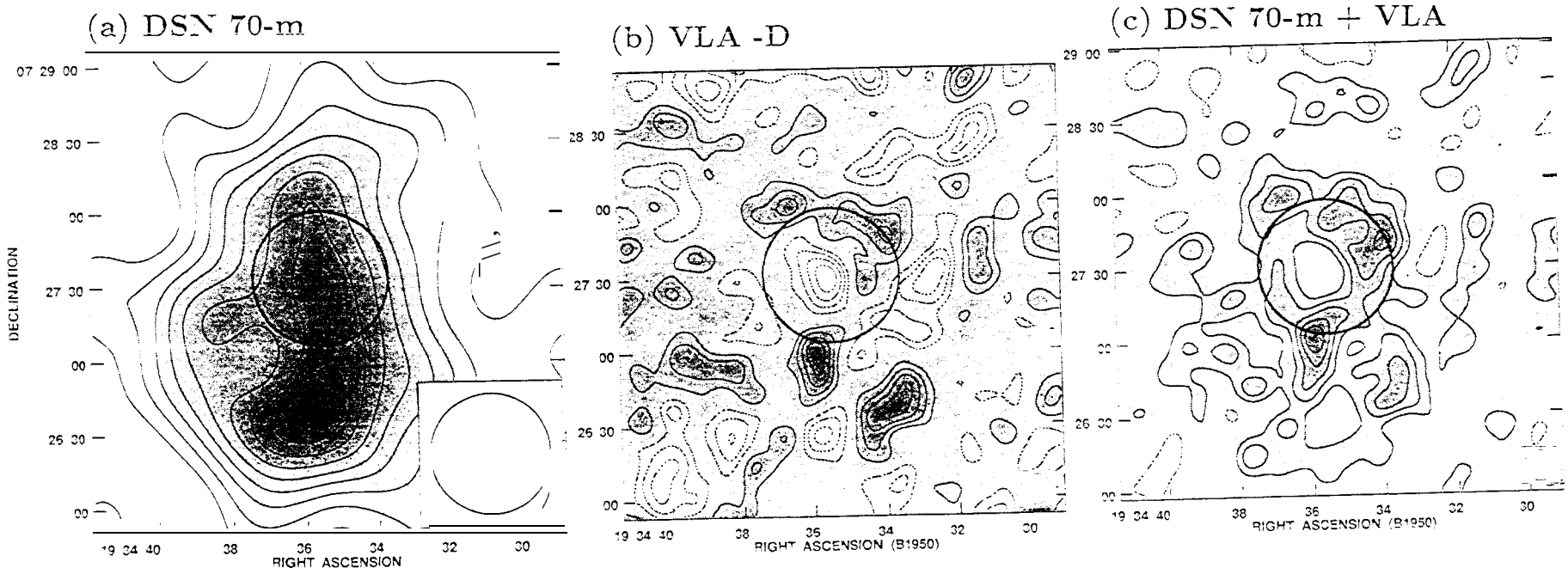
(a) DSN 70-m
(b) VLA -D
(c) DSN 70-m + VLA
DECLINATION
RIGHT ASCENSION
RIGHT ASCENSION (B1950)
RIGHT ASCENSION (B1950)

F. 5 2

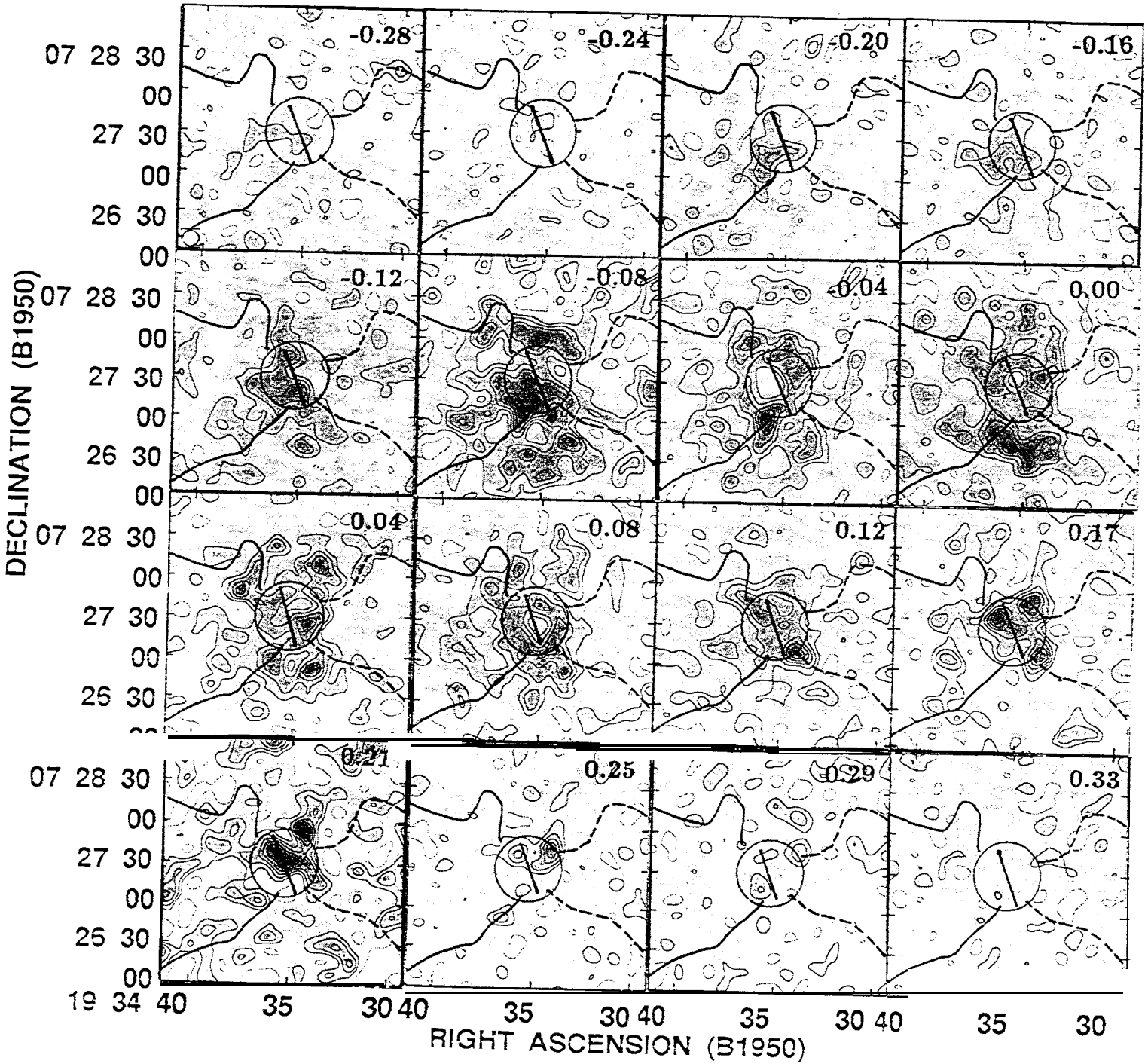
-0.28
-0.24
-0.20
-0.16
-0.12
-0.08
-0.04
0.00
0.04
0.08
0.12
0.17
0.21
0.25
0.29
0.33
07 28 30
00
27 30
00
26 30
00
19 34 40
35
30 40
35
30 40
35
30 40
35
30
DECLINATION (B1950)
RIGHT ASCENSION (B1950)

Fig 3

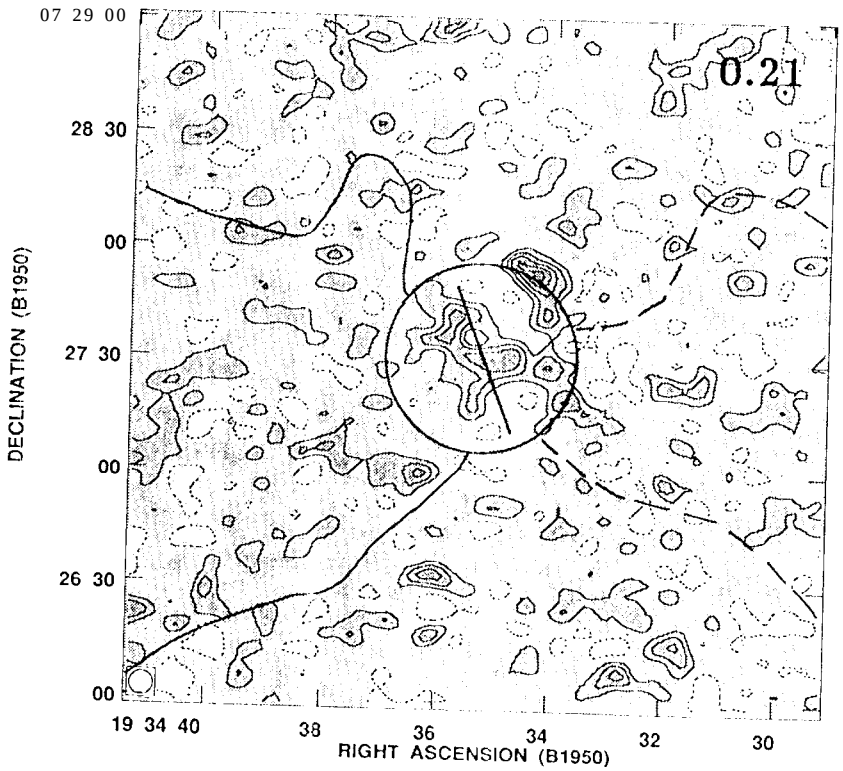
0.21
07 29 00
28 30
00
27 30
00
26 30
00
DECLINATION (B1950)
19 34 40
38
36
34
32
30
RIGHT ASCENSION (B1950)

Fig. 4

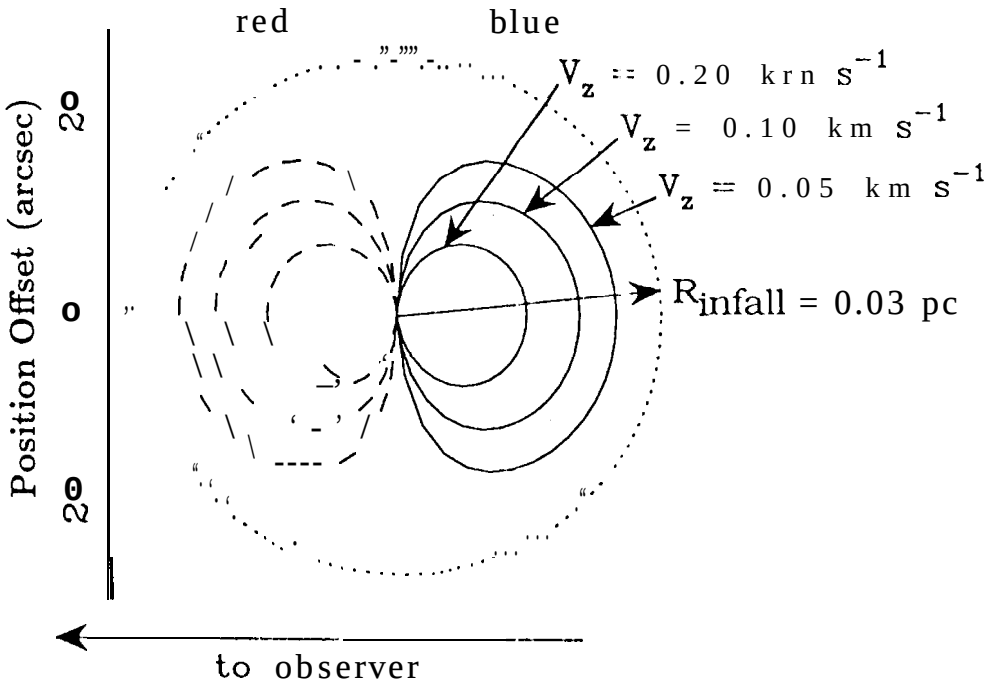
red
blue
V_z = 0.20 krn s^{-1}
V_z = 0.10 km s^{-1}
V_z = 0.05 km s^{-1}
R_{infall} = 0.03 pc
Position Offset (arcsec)
20
0
20
to observer

Fig. 5